Asian Journal of Chemistry; Vol. 37, No. 2 (2025), 413-430

ASIAN JOURNAL OF CHEMISTRY

https://doi.org/10.14233/ajchem.2025.33171

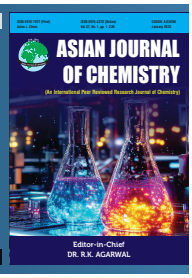

Experimental and Theoretical Analysis of 4-(4-(4,5-Dihydro-5-(4-isopropylphenyl)-1*H*-pyrazol-3-yl)phenyl)morpholine Molecule: Spectroscopy, NLO, Docking and Reactivity Studies

C. Bavani[1], Govindarajalu Kishore[1], Periyasamy Pritha[1], D. Bhakiaraj[2], S. Xavier[1,*] and S. Sebastian[1]

[1]Department of Physics, St. Joseph's College of Arts & Science (Autonomous), Cuddalore-607001, India
[2]Department of Chemistry, St. Joseph's College of Arts & Science (Autonomous), Cuddalore-607001, India

*Corresponding author: E-mail: puduvaixavier@gmail.com

Received: 10 December 2024; *Accepted*: 16 January 2025; *Published online*: 31 January 2025; AJC-21894

This study unveils the molecular structural and spectroscopic analysis of 4-(4-(4,5-dihydro-5-(4-isopropylphenyl)-1*H*-pyrazol-3-yl)-phenyl)morpholine (IPH) to determine its biological behaviour and stability through a DFT study. Theoretical calculations at the B3LYP/6-311G(d,p) level of the basis set and functional group have revealed unique and intriguing insights. Experimental UV-Vis, FT-IR and NMR analyses were carried out, predicting their functional group, mode of vibration and λ_{max} at 300 nm, which also correlated with the DFT studies. The donor-acceptor interactions of molecule have been clarified by executing the natural bond orbital (NBO). Potential energy distribution (PED) was used to identify the vibration mode. To evaluate the ^{1}H and ^{13}C NMR, the gauge independent atomic orbital (GIAO) approach is modified. The electronic transition of the molecule was established by applying the time-dependent density functional theory (TD-DFT) approach. It was found that the theoretical band gap was 4 eV, indicating that the molecule is reactive and stable. By examining the charge distribution and electrostatic potential of molecule, a significant data regarding its active area was revealed. Similarly, the electron-hole distribution was detected and the reactive sites were predicted through the electron localized function (ELF) and localized orbital locator (LOL) studies. The molecular docking was also performed to determine the biological behaviour of the molecules against prostate cancer and the inhibition rate and docking score were also calculated.

Keywords: Pyrazole, Optically active, Morpholine, Acceptor-donor, Electron-hole distribution.

INTRODUCTION

Morpholine (tetrahydro1,4-oxazine) is a heterocycle often used in therapeutic science because of its beneficial physico-chemical, natural and metabolic properties and its simple manufactured courses [1]. Fittingly subbed morpholines have been known for quite some time to have many organic activities, from pain relieving, antiinflammatory, cell reinforcement and antihyperlipidemic to antimicrobial, anti-neurodegenerative and anticancer activity [2]. This promising versatility has led to many morpholine-containing drugs in the market, with the potential to revolutionize cancer treatment.

The new medication plan, like little atoms in light of the pharmcologically appealing frameworks of thiazolidine (4-thiazolidinone) and pyrazole or pyrazoline, is a sensible and promising course in current restorative science. The substance approaches for the blend of thiazolidinedione and pyrazole-based subordinates and their pharmacological movement were depicted in various surveys. Nonetheless, the pyrazole/pyrazoline-thiazolidine-based forms as naturally dynamic mixtures are inadequately evaluated regarding the pharmacophore cross-over approach [3].

The newly manufactured investigations of the pyrazole-thiazolidines and related mixtures and organic examinations for their antitumor, antimicrobial, antiviral, antiparasitic and mitigating exercises permitted to distinguish the promising medication like mixtures. Hence, the pyrazole-thiazolidine-diones/thiazoles have been protected as inhibitors of necroptosis, VHR protein tyrosine phosphatase inhibitors, Pin1-tweaking compounds, compounds for regulating RNA restricting proteins and activators that support apoptotic BAX. Likewise, the pyrazole thiazolidinone half breeds have been read up for their likelihood to restrain the TNF-α-TNFRc1 connection as inhibitors of histone acetyltransferases and inhibitors of COX and ADAMTS-5 catalysts [4].

Pyrazole is a five-membered heterocyclic scaffold that possesses almost all types of pharmacological activities with two nitrogen atoms bound to each other and three carbon atoms. And due to its diverse topologies, they can create structures and used in mixing polymers, coordination structures and metal-normal designs [5].

The present study focuses on the synthesis of novel 4-(4-(4,5-dihydro-5-(4-isopropylphenyl)-1*H*-pyrazol-3-yl)phenyl)-morpholine, a biologically active compound. Its morphological, vibrational and spectroscopic studies were carried out through experimental and theoretical aspects. The experimental studies correlate to the theoretical outcomes, which supports the findings of the work [6,7]. Thus, an attempt is also made to analyze the structure of the compounds, bringing them down to the ground state [8]. With the use of second-order perturbation theory, the study additionally increased its reactions on electromagnetic spectrum radiation in non-orbital research. With the help of the data obtained at the ground state, the band gap, softness, hardness and stability of the molecules were calculated [9]. The molecular docking studies further analyzed the biological activity and verified that the studied docks more readily as compared than other compounds [10].

EXPERIMENTAL

Synthesis of 3-(4-isopropylphenyl)-1-(4-morpholinophenyl)prop-2-en-1-one: 1-(4-Morpholinophenyl)ethanone (5 mmol) dissolved in ethanol was added to 4-isopropylbenzaldehyde (5 mmol) and stirred well. Then, the mixture was cooled using an ice-cold water bath to 20 ºC and NaOH (15 mmol) solution was added. The reaction mixture was then agitated for 6 h. TLC was utilized to monitor the progress of the reaction. Once the reaction was completed, it was quenched with ice-cold water and kept overnight at room temperature. The solid settled was then filtered, washed with water and dried under vacuum to obtain 3-(4-isopropylphenyl)-1-(4-morpholinophenyl)prop-2-en-1-one.

Synthesis of 4-(4-(4,5-dihydro-5-(4-isopropylphenyl)-1*H*-pyrazol-3-yl)phenyl)morpholine: The synthesized intermediate chalcone, 3-(4-isopropylphenyl)-1-(4-morpholinophenyl)prop-2-en-1-one (1 mmol) was added to a round bottom flask containing hydrazine hydrate (3 mmol) and ethanol. The solution was stirred constantly for 8 h at room temperature and TLC technique was verified to evaluate the completion of the reaction. Following completion, ice was used to quench the reaction mixture and the separated solid was then filtered. The filtered solid was then washed thoroughly with distilled water and vacuum dried to obtain 4-(4-(4,5-dihydro-5-(4-isopropylphenyl)-1*H*-pyrazol-3-yl)phenyl)morpholine (**Scheme-I**).

Characterization: The UV-visible spectrum was recorded on a SpectraMax Plus 384 UV-visible spectrophotometer. The FT-IR spectrum was recorded on a Bruker FT-IR spectrometer using KBr pellet method. The ^{1}H and ^{13}C NMR spectra were recorded on a BRUKER AMX-400 NMR spectrometer at 293 K, operating with the frequencies of 400 MHz and 100 MHz, respectively, with $CDCl_3$ as solvent. The chemical shift values are reported in δ (ppm) referenced to TMS.

Computational details: The Gaussian 09 W program was used for the theoretical computations and the structure of the studied molecule were optimized by utilizing the B3LYP/6-311G(d,p) level of basis set and functional group [11,12]. The TED generated using VEDA software assigned different types of vibrations [13]. The molecule interaction study and bonding parameters were evaluated using the NBO analysis. Their band gap and reactivity nature were studied through the HOMO-LUMO calculation. The DFT/B3LYP method was used to optimized the geometry of the structures. The molecular electrostatic potential and the HOMO-LUMO calculations were also done on the optimized structures to ensure the band gap and reactivity nature of molecules. The AutoDock Vina software [14] was utilized to conduct docking studies to investigate the biological characteristics of the examined molecule with the prostate cancer protein (PDB ID 6XXO).

RESULTS AND DISCUSSION

4-Isopropylbenzaldehyde and 1-(4-morpholinophenyl)-ethanone were reacted in alkaline ethanolic method at 20 ºC to obtain 3-(4-isopropylphenyl)-1-(4-morpholinophenyl)prop-2-en-1-one. This synthesized chalcone compound was then treated with hydrazine hydrate in ethanol to obtain the final

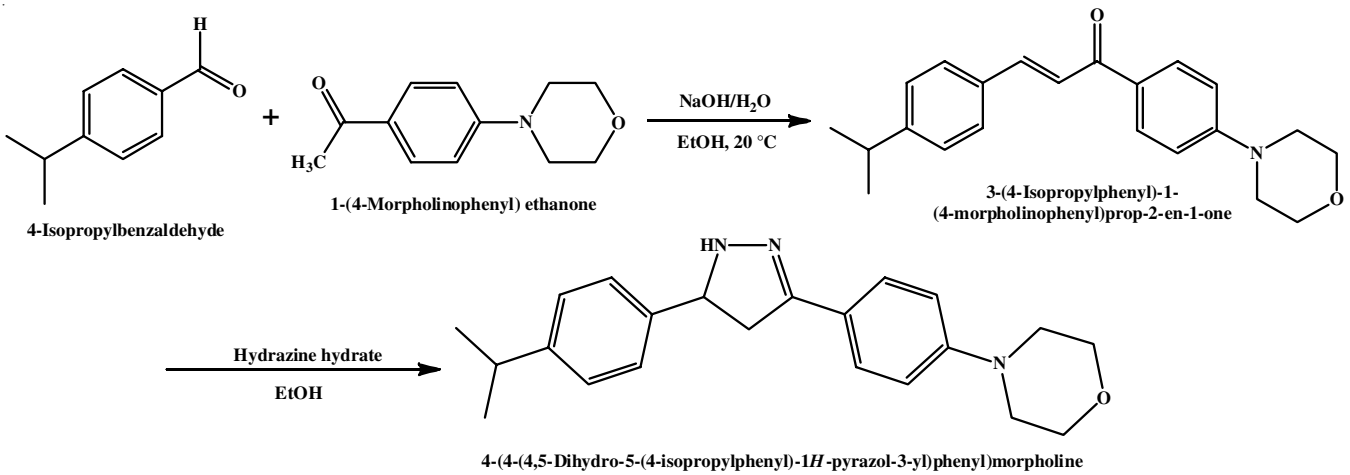

Scheme-I: Mechanism of synthesized 4-(4-(4,5-dihydro-5-(4-isopropylphenyl)-1*H*-pyrazol-3-yl)phenyl)morpholine

product, 4-(4-(4,5-dihydro-5-(4-isopropylphenyl)-1*H*-pyrazol-3-yl)phenyl)morpholine. The structure of the synthesized pyrazolyl compound was characterized with UV-Vis, FT-IR, ^{1}H NMR and ^{13}C NMR spectral studies.

Structural analysis: The structure of the target compound was optimized at the minimum energy level to determine their stability and structural properties through density functional theory (DFT) embedded in the Gaussian 09W computational software. Accordingly, the lowest energy state of 4-(4-(4,5-dihydro-5-(4-isopropylphenyl)-1*H*-pyrazol-3-yl)phenyl)-morpholine (IPH) was calculated using functional B3LYP and 6-311G(d,p) basis sets. The findings indicate that the energy of the optimal structure is -38 eV and the dipole moment is 2.083571 Debye. The optimized structure of the molecule is depicted in Fig. 1.

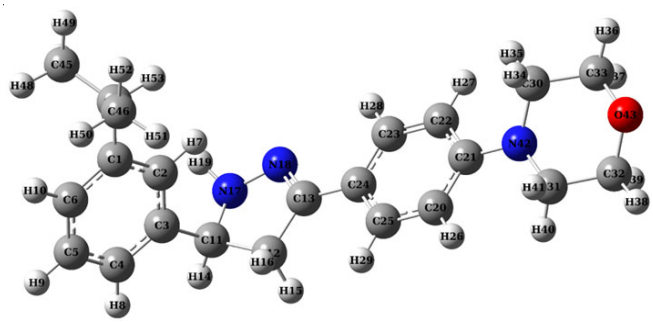

Fig. 1. Optimized structure of 4-(4-(4,5-dihydro-5-(4-isopropylphenyl)-1*H*-pyrazol-3-yl)phenyl)morpholine

Upon examining the bond lengths of the molecule, the C-C bond in pyrazole rings determines approximately 1.5 Å, whereas in benzene rings, it reveals between 1.39 Å and 1.4 Å. The C-O bond in morphine is approximately 1.42 Å; the C-H bond length ranges from 1.08 Å to 1.09 Å; the N-H bond measures 1.013 Å; the C-N bond is 1.48 Å in pyrazole and 1.46 Å in morphine; the N=C bond measures 1.28 Å, while the N-N bond length is 1.38 Å in pyrazole [15,16]. In the studied molecule, the molecule stabilizes itself in some areas, with the nearby functional groups taking the same bond lengths (Table-1). In certain regions, it deviates from the original structure. Likewise, the C-C, N-H and C-O take the same value in all the regions of the molecule,

TABLE-1
GEOMETRICAL ANALYSIS OF TITLED MOLECULE

Bond length	Values (Å)	Bond angle	Values (°)
N17-N18	1.405	C13=N18-N17	109.4
N18=C13	1.305	C11-C12-C13	102.4
C1-C6	1.406	C25-C20-C21	102.9
C32-O43	1.420	C31-N42-C30	113.0
C30-H35	1.087	C32-O43-C33	110.7
C1-C2	1.400	C1-C44-C45	112.0
C44-H53	1.095	H47-C45-H48	107.9

but in case of the C=C, there are more significant deviations of 0.02 Å at C-C since it is attached to the nitrogen atom. There are also fewer observable deviations in C3-C4 and C11-C3 bonds to the level of 0.01 Å on stabilizing itself with the neighbouring atoms. In contrast C-N, at one region C30-N42, was observed to be 1.4 Å and instead, at C2-C3, it elongated with the values of 0.1 Å. Similarly, the N-N takes neutral values with 1.388 Å and retains its original bond lengths in all other molecule regions [17,18]. The geometrical values was tabulated in Table-2.

Vibrational analysis: The vibrational analysis of the target molecules was carried out by Gaussian 09W software employing B3LYP/6-311G (d,p) keysets. The target molecule contains 53 atoms, which exhibits 153 modes of vibrations by non-linear equation (3n-6) [19]. The molecule point group symmetry was C1, perfect with the reference data. The molecule possesses different vibrational modes *viz*. stretching, bending, twisting, inplane and out-of-plane vibrations.

CH vibrations: The molecule consisted for two six membered rings constituting a high flow of energy. The CH vibrations in the molecule were found in the dimethylbenzenamine, pyrazole and morphine rings. The CH vibrations are around 3077, 3075, 3073, 3051 and 3035 cm^{-1}. The sharp peak was observed at 3071 and 3052 cm^{-1} and all the CH vibrations corresponded to the stretching mode [20]. Similarly, the CH vibrations were found around 3090, 3083 and 3153 cm^{-1}, which also greatly agreed with the experimental FT-IR analysis. The theoretical vibrational values are tabulated in Table-3.

C=C vibrations: The C=C vibration generally appears in the ring moiety at 1586 and 1544 cm^{-1}, which agrees with the experimental range, however, the presence of adjacent pyrazole

TABLE-2
OPTIMIZED TABLE OF TITLED MOLECULE

Bond length	Value	Bond length	Value	Bond length	Value	Bond length	Value
C1-C2	1.3964	C11-C17	1.4848	C22-C27	1.083	C32-C39	1.1004
C1-C6	1.4012	C12-C13	1.5196	C23-C24	1.4083	C32-C43	1.4201
C1-C44	1.5224	C12-C15	1.0958	C23-C28	1.083	C33-C36	1.0914
C2-C3	1.4008	C12-C16	1.0913	C24-C25	1.3982	C33-C37	1.1005
C2-C7	1.0855	C13=C18	1.2881	C25-C29	1.0841	C33-C43	1.4209
C3-C4	1.3958	C13-C24	1.4619	C30-C33	1.5242	C44-C45	1.5392
C3-C11	1.5207	C17-C18	1.3882	C30-C34	1.1029	C44-C46	1.5397
C4-C5	1.3936	C17-C19	1.0128	C30-C35	1.0893	C44-C53	1.0957
C4-C8	1.0855	C20-C21	1.4028	C30-C42	1.469	C45-C47	1.0928
C5-C6	1.3902	C20-C25	1.3931	C31-C32	1.527	C45-C48	1.094
C5-C9	1.0847	C20-C26	1.0815	C31-C40	1.0922	C45-C49	1.094
C6-C10	1.0847	C21-C22	1.4121	C31-C41	1.1037	C46-C50	1.0941
C11-C12	1.5517	C21-C42	1.4074	C31-C42	1.4603	C46-C51	1.0928
C11-C14	1.0919	C22-C23	1.3803	C32-C38	1.0915	C46-C52	1.0941

TABLE-3
VIBRATIONAL TABLE ASSIGNMENT OF TITLED MOLECULE

Mode No.	Unscaled values	Scaled values	IR_{Int}	TED assignments
1	3591.6679	3448.001184	17.7577	
2	3205.3806	3077.165376	8.8434	ν CH (92)
3	3202.7071	3074.598816	22.4781	
4	3184.8748	3057.479808	40.1817	
5	3181.5177	3054.256992	17.9096	
6	3171.3917	3044.536032	26.6791	N CH (99)
7	3165.7133	3039.084768	29.8084	
8	3159.9760	3033.576960	9.9109	
9	3153.2494	3027.119424	2.8634	ν CH (100)
10	3117.8863	2993.170848	11.9925	
11	3112.7192	2988.210432	52.8789	
12	3109.9744	2985.575424	35.9458	
13	3090.4095	2966.793120	41.005	ν CH (93)
14	3086.9877	2963.508192	25.5115	
15	3084.9163	2961.519648	22.5079	
16	3083.4208	2960.083968	83.8535	ν CH (93)
17	3082.4113	2959.114848	18.9126	
18	3075.0992	2952.095232	0.0605	ν CH (99)
19	3061.4622	2939.003712	34.2177	ν CH (91)
20	3020.1435	2899.33776	23.6639	ν CH (95)
21	3014.0222	2893.461312	37.8414	ν CH (90)
22	3009.6335	2889.248160	30.5282	
23	3004.0995	2883.935520	13.4374	ν CH (95)
24	2999.1826	2879.215296	107.2556	ν CH (91)
25	2993.0081	2873.287776	16.814	ν CH (91)
26	2946.5971	2828.733216	100.4336	
27	2938.3333	2820.799968	49.3135	ν CH (88)
28	1653.0017	1586.881632	138.8278	ν CC (50) + β CCC (10)
29	1642.9506	1577.232576	19.8208	
30	1626.7822	1561.710912	5.4442	
31	1612.3795	1547.884320	35.8549	ν NC (45)
32	1580.7787	1517.547552	2.4133	
33	1563.8763	1501.321248	135.1705	
34	1547.7988	1485.886848	12.7881	
35	1542.1702	1480.483392	7.4029	
36	1532.6695	1471.362720	13.0331	
37	1530.8070	1469.574720	37.0688	
38	1529.8143	1468.621728	3.8547	β HCH (37) + τ HCCC (33)
39	1528.1458	1467.019968	0.0437	β HCH (64)
40	1522.4516	1461.553536	8.5083	β HCH (70)
41	1520.7263	1459.897248	7.2961	
42	1515.8107	1455.178272	7.8978	
43	1513.5336	1452.992256	1.5711	
44	1489.5622	1429.979712	12.4812	
45	1466.4175	1407.760800	25.8116	ν CC (44) + β HCC (16)
46	1455.0338	1396.832448	11.2656	β HCC (20) + β HCH (20) + γ CHHH (38)
47	1453.9449	1395.787104	2.9324	β HCC (22) + γ CHCH (10) + τ HCOH (15)
48	1436.7778	1379.306688	8.6336	
49	1432.9352	1375.617792	46.5881	
50	1419.2607	1362.490272	5.2535	β HCC (22) + γ CHCH (10) + τ HCOH (15)
51	1413.8514	1357.297344	2.3367	
52	1403.7876	1347.636096	36.3887	
53	1394.9478	1339.149888	48.505	
54	1393.1408	1337.415168	16.7375	τ HCNH (17) + τ HCOC (11) + γ CHCH (22)
55	1379.6959	1324.508064	38.6548	
56	1367.2077	1312.519392	2.8789	ν CC (10) + β HCC (70)
57	1366.9003	1312.224288	0.5497	
58	1361.6430	1307.177280	29.9034	
59	1356.4623	1302.203808	26.6938	β HCC (22)
60	1334.8736	1281.478656	0.5704	

61	1324.6906	1271.702976	21.2218	
62	1323.0931	1270.169376	5.4443	β HCO (67)
63	1310.1146	1257.710016	4.732	ν CC (21)
64	1298.4990	1246.559040	36.0948	β HCO (42) + τ HCNC (10)
65	1275.0146	1224.014016	12.315	ν CC (37)
66	1269.1472	1218.381312	174.645	γ CCCH (14)
67	1263.3206	1212.787776	106.3425	γ CCCH (15) + τ HCCC (11)
68	1244.9944	1195.194624	7.4398	
69	1240.6419	1191.016224	52.8202	
70	1223.2718	1174.340928	10.3909	β HCC (17)
71	1222.4551	1173.556896	10.5141	β HCC (43)
72	1198.5376	1150.596096	5.3777	
73	1195.9992	1148.159232	13.129	
74	1186.7355	1139.266080	0.8629	
75	1159.8464	1113.452544	2.632	N CH (34)
76	1140.2953	1094.683488	23.5967	γ CCNH (10) + γ CCOH (28) + τ CCOC (12)
77	1132.8874	1087.571904	1.29	N CC (36) + γ CHCH (17)
78	1132.4354	1087.137984	1.4692	N CC (36) + γ CHCH (17)
79	1109.4381	1065.060576	50.4864	N CC (13) + N OC (36) + γ CCOH (10)
80	1087.0778	1043.594688	28.6028	N OC (29) + γ CCNH (14)
81	1086.4547	1042.996512	11.9061	β CCC (10) + β HCC (10) + γ CHCH (16)
82	1078.7016	1035.553536	0.8264	
83	1068.2060	1025.477760	6.3796	N CC (13)
84	1061.8412	1019.367552	80.4922	
85	1040.1384	998.532864	13.7147	N CC (20)
86	1036.7159	995.247264	11.1246	
87	1031.1632	989.916672	0.9884	β CCC (39)
88	1025.8531	984.818976	4.5549	
89	1013.5084	972.968064	1.6192	
90	1010.6069	970.182624	8.5426	
91	1006.3507	966.096672	43.7196	N NC (17) + N CC (11)
92	980.1935	940.985760	0.0285	N CC (23) + γ CHCH (16) + τ HCCC (17)
93	978.4818	939.342528	2.8554	N NC (30) + N CC (18)
94	972.3696	933.474816	5.0032	τ HCCH (74) + τ HCCC (12)
95	956.5111	918.250656	1.1912	β HCC (47) + γ CCCH (10)
96	946.0689	908.226144	0.104	γ CCCH (86)
97	940.3135	902.700960	3.2931	γ CCCH (72)
98	937.4886	899.989056	25.841	
99	931.9539	894.675744	78.322	
100	923.4240	886.487040	4.7719	N CC (30)
101	877.9151	842.798496	2.8673	
102	870.4015	835.585440	23.5764	τ HCCN (11) + γ CCNH (12) + γ CCOH (12)
103	862.9011	828.385056	31.4168	
104	845.0474	811.245504	10.7344	N CC (27)
105	844.4802	810.700992	18.724	τ HCCN (11) + τ HCCC (53)
106	833.5327	800.191392	52.1414	
107	831.1966	797.948736	5.0692	γ CCCH (37)
108	822.6523	789.746208	9.5887	
109	758.8486	728.494656	2.1428	
110	755.5289	725.307744	6.6951	
111	738.7324	709.183104	18.6603	
112	731.6614	702.394944	6.6882	
113	670.1352	643.329792	10.8368	β CCC (32)
114	664.5701	637.987296	12.3219	
115	657.3327	631.039392	8.1942	τ CCCC (32)
116	632.4880	607.188480	65.078	β CCC (32) + τ CNNC (11)
117	589.0752	565.512192	0.8878	β CCC (21) + γ CCCC (11)
118	587.5587	564.056352	145.9041	
119	553.4697	531.330912	4.8578	β CCO (27)
120	547.2311	525.341856	124.3356	γ NCNH (38) + γ CCCC (27)
121	512.0003	491.520288	5.6217	τ CCNN (25)
122	497.5809	477.677664	55.927	

123	483.8236	464.470656	13.8465	
124	475.1887	456.181152	12.4775	β CCC (10)
125	469.6759	450.888864	1.6008	
126	433.1241	415.799136	9.4954	β HCN (23) + τ HCNC (13) + γ CHCH (20) + τ HCOC (10) + τ CCCC (60)
127	431.1038	413.859648	8.8322	NCC (11) + β CCN (11) + β CCO (12)
128	416.6848	400.017408	1.3069	
129	411.8108	395.338368	0.7277	
130	381.8525	366.578400	1.1395	
131	349.0595	335.097120	1.3074	β CCC (11)
132	328.6249	315.479904	0.1351	
133	317.0543	304.372128	3.9625	N CH (99) + β CCC (21) + β CCN (11)
134	310.2894	297.877824	0.2962	N CC (21) + β CCC (15)
135	277.3256	266.232576	28.8796	τ CCNN (10) + γ CCCN (12)
136	262.4943	251.994528	3.0931	
137	247.6638	237.757248	9.4034	
138	235.5815	226.15824	2.44	
139	224.0243	215.063328	0.6277	τ HCCC (55)
140	217.8009	209.088864	0.9809	
141	206.0775	197.834400	0.2623	β CCC (12)
142	168.1953	161.467488	1.1858	β CNC (12)
143	144.7434	138.953664	0.5463	
144	134.0768	128.713728	0.9962	β CCC (10)
145	120.8295	115.996320	0.0974	
146	99.2906	95.318976	3.6069	β CCC (17) + β CCN (11)
147	72.0501	69.168096	0.3935	β CCC (12) + τ CNCC (26)
148	69.8604	67.065984	2.7121	
149	42.3491	40.655136	0.5468	
150	38.5319	36.990624	0.0937	τ CCCC (28) τ CCCN (11) + γ CCCN (11)
151	30.7815	29.550240	0.3726	τ CCCN (10)
152	22.5752	21.672192	0.0736	
153	14.9934	14.393664	0.0439	

slightly constrains the wavelength. The C=C was observed at 1653 cm^{-1} and the bending vibration of C-C-C was observed at 1031 cm^{-1}, matched and fitted with the experimental FT-IR analysis [21]. The experimental FT-IR and theoretical spectra are shown in Fig. 2.

Experimental FT-IR studies: In the FT-IR spectrum of the synthesized compound, a strong absorption observed at 1513 cm^{-1} is due to C=N stretching frequency. The absorptions observed at 2977 cm^{-1} and 2923 cm^{-1} are due to aromatic C-H stretching frequencies. The absorptions observed at 2849 cm^{-1} is due to aliphatic C-H stretching frequency. The absorption observed in the range of 1177 cm^{-1} is due to C-O stretching frequency and the absorption observed in the range of 1231 cm^{-1} and 1247 cm^{-1} are due to C-N stretching frequencies. The absorption frequencies in the FT-IR spectrum for the synthesized compound confirm the formation of the desired product.

UV-vis studies: The UV-vis analysis was employed to determine the transition state of molecules in both experimental

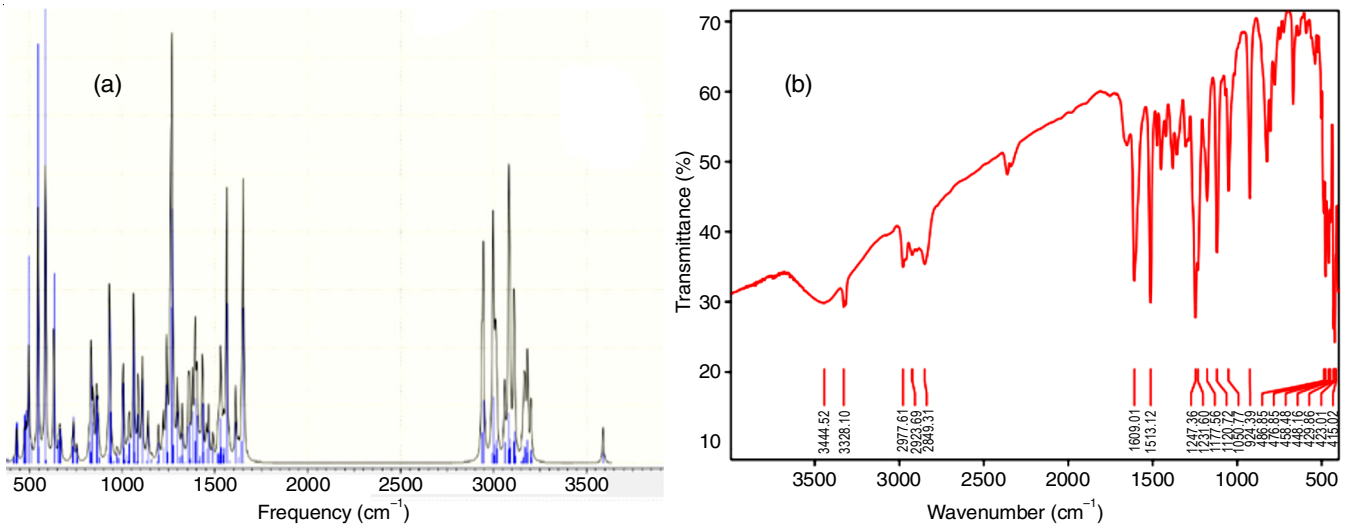

Fig. 2. Theoretical (a) and Experimental (b) FT-IR spectral analysis of titled molecule

and theoretical ways. The TD-SCF calculation used DMSO as a solvent in the gas and solvent phases [22]. The experimental UV-vis spectra give a broad peak at 300 nm. Their theoretical λ_{max} values were observed at 323 nm. A slight shift in the theoretical values was due to the exchange-correlation functions. Fig. 3a-b depict the absorbance spectra in which aromatic rings in the molecules show absorbance in this region due to similar $\pi \rightarrow \pi^*$ transitions within the aromatic ring. The absorbance at 300 nm for the title molecule exhibits $\pi \rightarrow \pi^*$ of the heteroaromatic compounds in the ring structure, including nitrogen and oxygen [23]. These outcomes showed that the synthesized molecule is the UV-vis active species and acted as optically stable compound.

Band gap analysis: The theoretical band gap was derived from the Density of states (DOS) analysis computed from the GaussSum software. The band gap obtained from the Tauc plot was around 4.28 eV and the band gap obtained from the DOS was 4.2 eV. Both the experiment and theoretical energy gaps complement each other are shown in Fig. 4a-b. The energy gap at 4.2 eV gives the stability of the synthesized molecule. The present results are more similar with those of Bhavani *et al.* [24], who reported the band gap of about 3.7 eV of *p*-hydroxyacetanilide crystals. These values suggest that the molecule has the potential to absorb UV light while remaining transparent to visible light, which could be advantageous in photoprotective or UV-blocking applications. The value around 4.2 eV shows the photocatalytic application of the molecule, which was also a great match with the UV-vis spectra and the theoretical HOMO-LUMO analysis.

^{1}H NMR studies: In ^{1}H NMR spectrum of the synthesized compound, the triplet signal appeared at δ 3.30-3.33 ppm is due to the four numbers of two sets of N-CH_2 protons of morpholine ring. Similarly, the signal appeared at δ 3.86 ppm is due to four numbers of two sets of O-CH_2 protons of the morpholine ring. The signal observed at δ 1.38-1.45 ppm is due to the six protons of two CH_3 groups at the isopropyl part attached to the

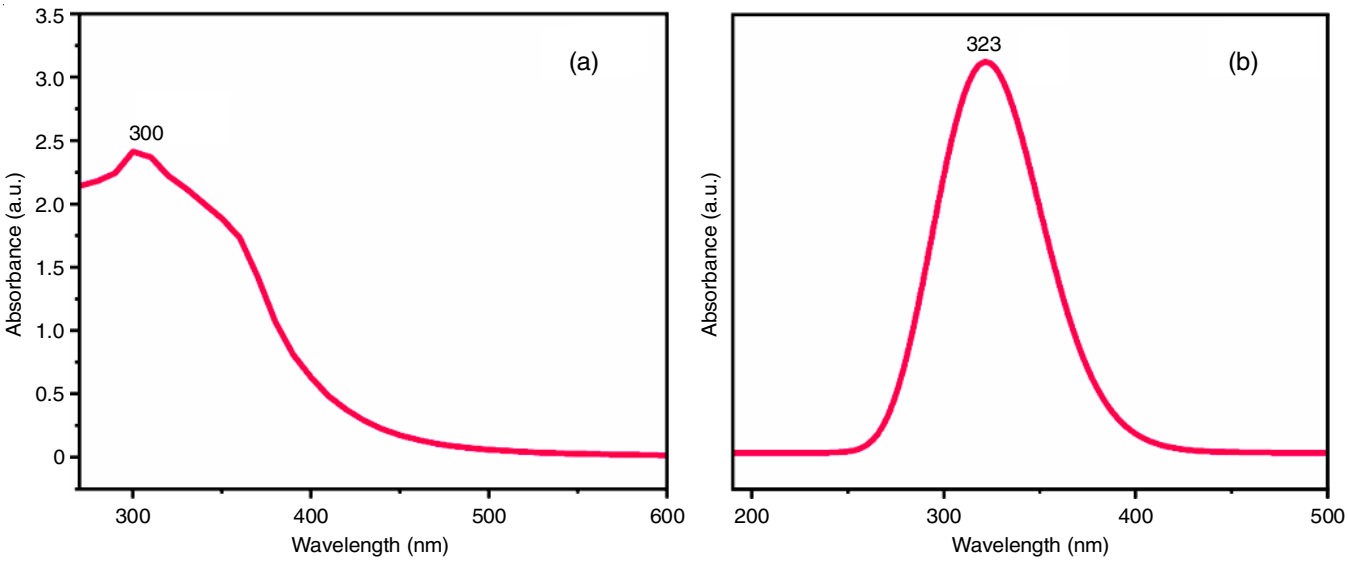

Fig. 3. (a) Experimental absorbance spectra and (b) theoretical absorbance spectra of titled molecule

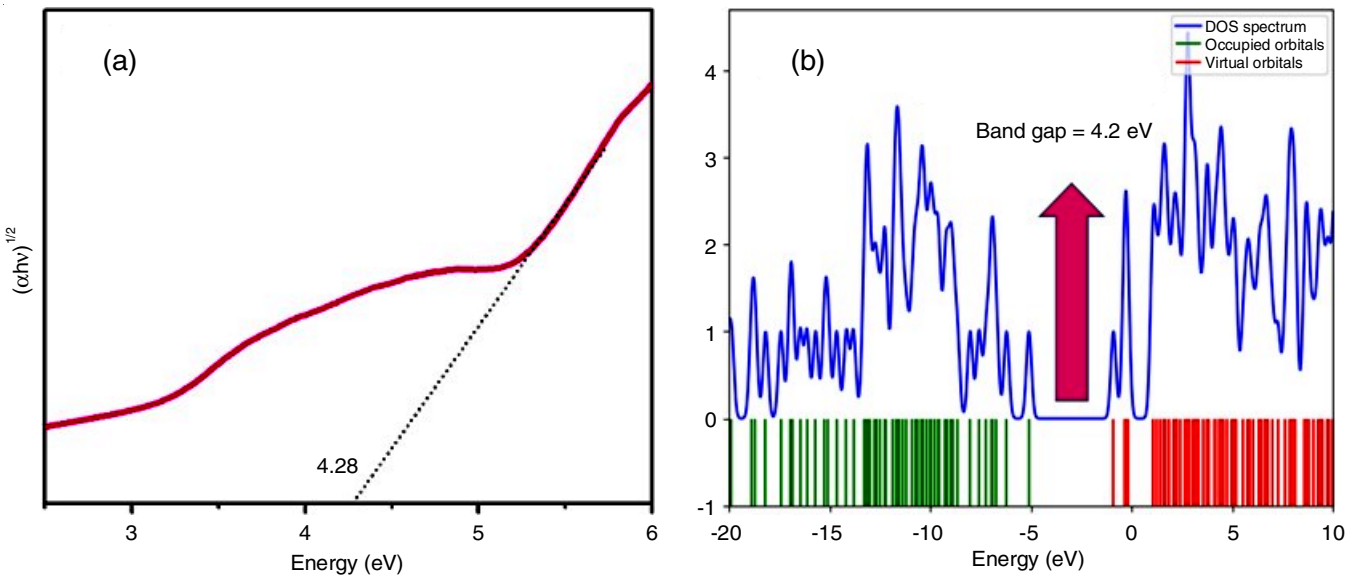

Fig. 4. Tauc plot obtained from UV-vis absorbance (a) and theoretical DOS spectra (b)

aromatic ring. The signal observed at δ 2.97-3.03 ppm is due to the proton of the -CH- junction group at the isopropyl part attached to the aromatic ring. The signal observed at δ 3.19-3.22 ppm is due to the proton at the C-5 position of the pyrazolyl ring and the signal observed at δ 3.39-3.41 ppm is due to the two protons at the C-4 position of the pyrazolyl ring. The signal observed at δ 4.83 ppm is due to the N-H proton at the pyrazolyl ring. The aromatic protons of the phenyl rings appeared in the range of δ 6.83-8.02 ppm. The ^{1}H NMR data confirms the formation of the synthesized title compound.

^{13}C NMR spectrum: In ^{13}C NMR spectrum, the signal observed at δ 48.70 ppm is due to the two carbons attached to the nitrogen atom in the morpholine ring. Similarly, the signal observed at δ 66.78 ppm is due to the two carbons attached to the oxygen atom in the morpholine ring. The carbon signal observed at δ 14.64 and 14.82 ppm is due to the two methyl carbons at isopropyl attached to the aromatic ring. The signal observed at δ 41.44 ppm is due to the -CH- junction carbon at the isopropyl part attached to the aromatic ring. The signal observed at δ 47.35 ppm is due to the -CH_2 carbon at the C-4 position of the pyrazolyl ring and the signals observed at δ 63.49 and 63.59 ppm are due to the two carbons at the C-5 and C-3 positions of the pyrazolyl ring, respectively. The aromatic carbons of two phenyl rings appeared in the δ 114.71-127.47 ppm range and the aromatic *ipso*-carbons appeared at δ 152 and 158 ppm. The ^{13}C NMR data for the synthesized compound further confirms the formation of the target compound.

Mulliken atomic charges and Fukui function: The title molecule shows more electrophilic in all the carbon atoms in the benzene and in pyrazol rings, taking a more electrophilic nature with the values of 0.2 amu (Fig. 5). Nitrogen and carbon atoms attached to carbon and nitrogen show the negative values thus, this molecule exhibits a greater affinity for positive charges. Apart from these deviations, many carbon atoms attached to the morpholine and pyrazole rings change the polarity, taking the primary positive values [25]. The negative values indicate the presence of nitrogen and oxygen compounds, which shows that these atoms are nucleophilic in nature [26]. The negative and positive values may vary according to the chemical composition and the functional groups. In present study, the atoms exhibited in hostile regions indicate the electron-rich region in Fig. 5, moreover, the negative values denote the stability of the compounds.

fk^{+}: The reduction in order of local atoms for fk^{+} are listed as: C21 > C13 > C23 > C33 > C6 > C15 > C1 > C22 > C4 > C3 > C2 > C11 > C5 > C20 > C24 > C30 > C31 > C12 > C44 > C46 > C45. The H19 atom in the pyrazole gives a higher charge than the other atoms. The H19 is electron-deficient and acts as a nucleophilic nature. The H19 was also found to have higher values in Mulliken charge analysis.

fk^{-}: The carbon atoms with a decrease in charge denoted as electrophilic was in the order as C21 < C13 < C32 < C33 < C11 < C31 < C1 < C30 < C23 < C2 < C4 < C3 < C6 < C22 < C5 < C25 < C24 < C20 < C12 < C44 < C46 < C46 < C45. The C21 atom is more electron donor region and has nucleophilic attack [27].

Δfk: The Δfk shows both positive as well as negative charges, which, as a result, shows the stability and active regions of the molecule. The C45 and C46 were observed to be more negative, which makes them prone to the electrophilic attack.

Molecular electrostatic potential (MEP): According to the contour plot and MEP map of the title molecule, the green colour has zero potential, the blue colour is electron-deficient, the yellow colour is slightly electron-rich and the red colour is electron-rich. The order of potential increases is red < orange < yellow < green < blue. The polarity of the molecule increases in proportion to the number of red/blue differences [28]. The molecule is primarily non-polar if the surface is mainly white or lighter colour shades. The MEP colour contour shows the hostile regions are electrophilic and mainly cover the nitrogen and oxygen atoms (N18, N17, N42 and O43) as shown in Fig. 6. The positive region is called the nucleophilic region, which is found over the hydrogen atoms and indicates that all hydrogen atoms have the most potent attraction, whreas N and O atoms indicate strong repulsion. The electron density plot for the molecule is uniformly distributed [29]. From these results, the nitrogen, oxygen and sulfur atoms are the dominant species for the electrostatic potential and help the stability of molecule.

HOMO-LUMO reactivity analysis: The GaussView 5.0 software package gathers the HOMO and LUMO values of the molecule. The energy gap of the compound was calculated to assess its mobility, with the estimated value being 4.2 eV. Based on these findings, it was determined that the molecule demonstrates a comparable effect and possesses moderate reactivity and stability [30]. The electron affinity, electronegativity and chemical potentials were calculated and tabulated in Table-4. From Fig. 7, the mapping was found in the carbon atoms and the pyrazole ring and the nitrogen, oxygen and sulfur atoms are electron-rich regions.

TABLE-4
HOMO-LUMO REACTIVE
DESCRIPTOR OF TITLED MOLECULE

Parameters	Values
E_{HOMO} (eV)	-5.10
E_{LOMO} (eV)	-0.90
$E_{HOMO} - E_{LOMO}$ gap (eV)	4.20
Ionization potential (I)	5.10
Electron affinity (A)	0.90
Electronegativity (χ)	2.1
Chemical potential (μ)	-3
Global hardness (η)	0.238
Global softness (S)	3
Electrophilicity index (ω)	9.45

NLO studies: The hyperpolarizability, linear polarizability and dipole moment were calculated using the B3LYP/6-311G-(d,p) level theory in order to determine the organic NLO property of the material [31]. The total molecular dipole moment was found to be 0.82D, which was half the value of urea (μ = 1.37 D). The total polarizability of the compound was found to be 31.672 Å^3. The dipole moment of the synthesized molecule (1.762279 D) is comparatively smaller than the dipole moment of urea, which denotes that the target molecule has moderate polarity. However, the total hyperpolarizability (β_{total}) is 1343.53948 a.u., much higher than the urea. The values from

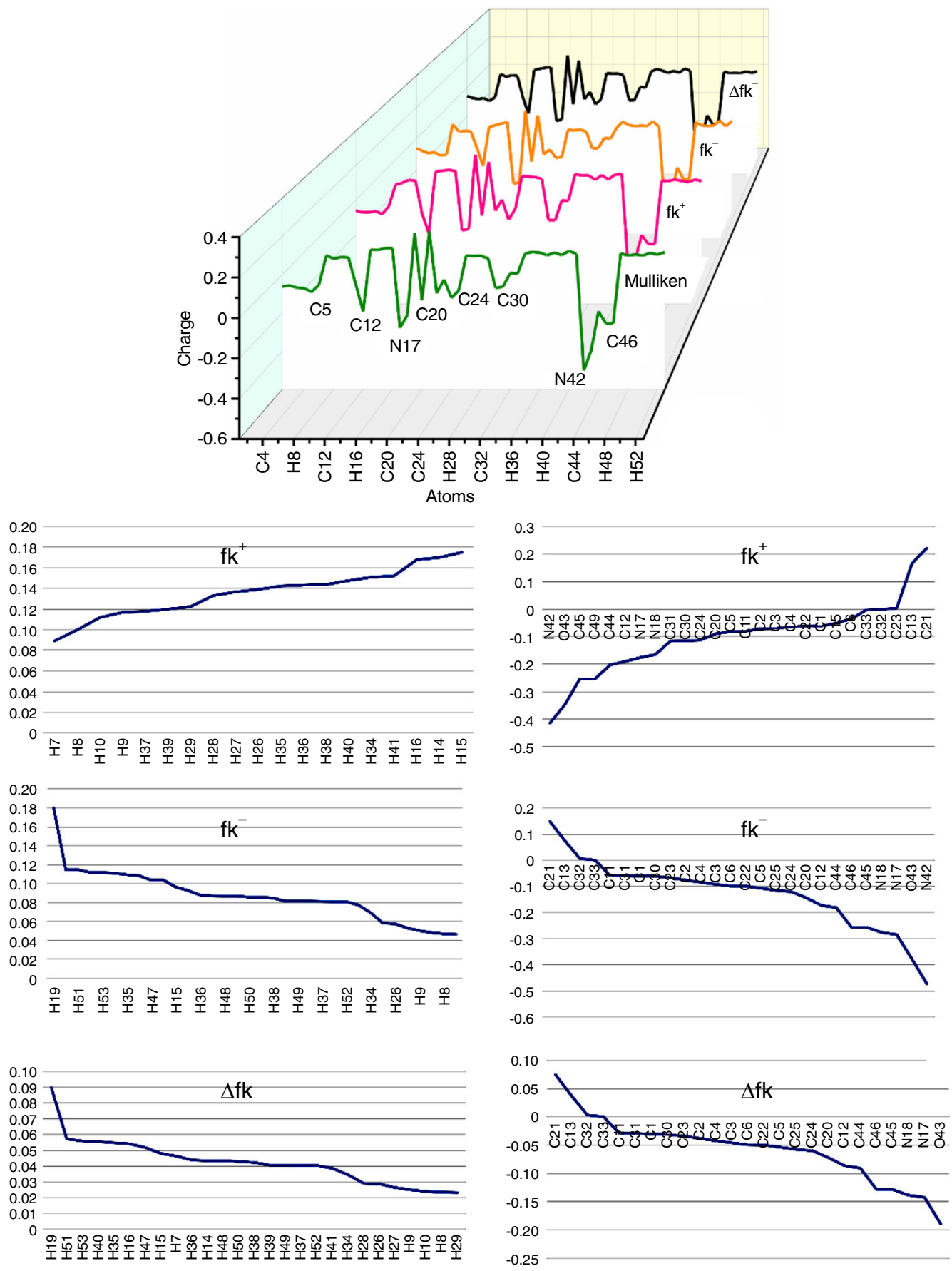

Fig. 5. Mulliken and Fukui analysis of titled molecule

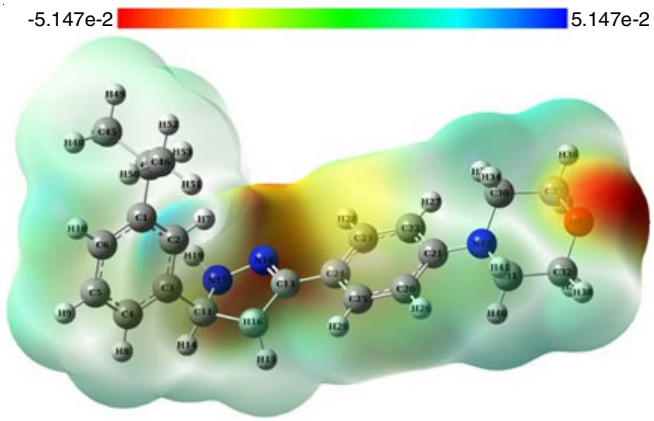

Fig. 6. Molecular electrostatic potential of titled molecule

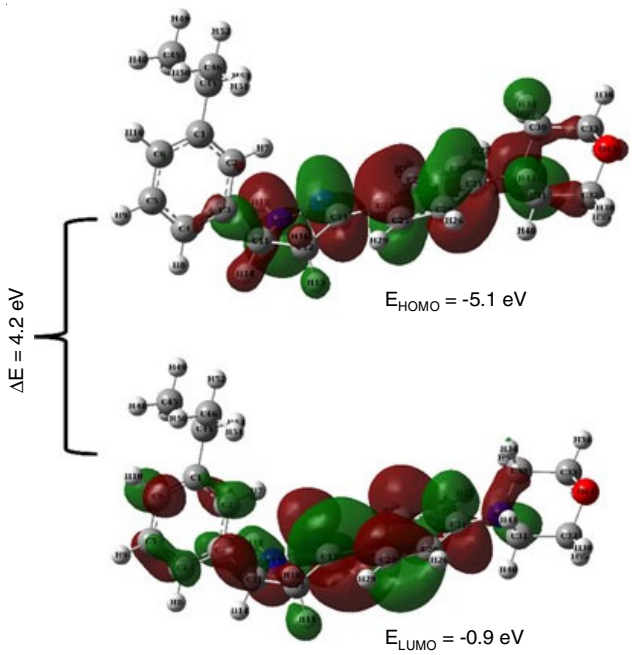

Fig. 7. HOMO-LUMO mapping of titled molecule

Table-5, indicate that the molecule has potential applications in optoelectronics and photonic technologies [32].

TABLE-5
DIPOLE MOMENT (μ), POLARIZABILITY (α) AND HYPER POLARIZABILITY (β) VALUES OF THE MOLECULE

Component	Value	Component	Value
α_{xx}	395.5265	β_{yyy}	125.1817
α_{xy}	-36.1939	β_{xxz}	-68.1700
α_{yy}	233.6533	β_{xyz}	-47.9234
α_{xz}	3.322305	β_{yyz}	-41.0816
α_{yz}	11.96036	β_{xzz}	-85.6613
α_{zz}	221.1104	μ_x	0.463282
β_{xxx}	1343.539	μ_y	0.233094
β_{xxy}	-172.904	μ_z	-0.63484
β_{xyy}	21.4882		

Natural bond orbital: The transfer of occupied orbital to unoccupied orbital was calculated through this study. For the target molecule, through orbital overlap between σ(C-C) and σ*(C-C), the intermolecular charge transfer (ICT) in the electron acceptor molecule helped to stabilize the molecule. The NBO orbitals depend on the strength of the interactions between electron donors, which raises the overall conjugation level of the system. The donor-acceptor perturbation energy of π(C1-C2) → π* (C5-C6) has 19.2 Kcal/mol, whereas the donor-acceptor perturbation energy of π(C3-C4) → π*(C1-C2) and π*(C5-C6) have values of 18.69 and 21.3 Kcal/mol [33].

The C-C and anti-C-C bonds in the ring system have developed the intramolecular hyperconjugation interaction for σ and π electrons. It is further noticed that the occupancy falls around ~ 0.01-0.31 e, for the bond contains carbon, carbon bonded with the neighboring nitrogen atoms (N20). The π (C13-N18) → π*(C13-N18), π*(C24-C25) of 0.24 and 10.22 Kcal/mol. The highest electron donor was observed in the π (C20-C21) → π* (C24-C25), with a 22.35 Kcal/mol value. The NBO results are tabulated in Table-6.

Electron-hole analysis: The experimental UV-vis spectrum has a peak at 300 nm, indicating the active electron mobility of the molecule. The experimental studies revealed that the molecule has different transition states. The electron-hole analysis was carried out by the Multiwfn software and their three excitations were computed. The various transitions are depicted

TABLE-6
NBO TABLE OF TITLED MOLECULE

Donor NBO (i)	Bond type	Electron density	Acceptor NBO (j)	Bond type	Electron density	kcal/mo	l a.u.
C1-C2	σ	1.97063	C1-C6	σ*	0.02727	3.66	1.25
C1-C2	σ	1.97063	C1-C44	σ*	0.03171	2.46	1.1
C1-C2	σ	1.97063	C2-C3	σ*	0.02604	4.43	1.25
C1-C2	σ	1.97063	C2-H7	σ*	0.01683	1.49	1.13
C1-C2	σ	1.97063	C3-C11	σ*	0.03717	3.49	1.09
C1-C2	σ	1.97063	C6-H10	σ*	0.01592	2.61	1.13
C1-C2	σ	1.97063	C44-C45	σ*	0.01746	0.63	1.05
C1-C2	σ	1.97063	C44-C46	σ*	0.01765	0.57	1.05
C1-C2	σ	1.97063	C3-C4	σ*	0.02412	22.95	0.28
C1-C2	π	1.65776	C5-C6	π*	0.32384	19.2	0.27
C1-C2	π	1.65776	C44-C45	σ*	0.01746	2.76	0.61
C1-C2	π	1.65776	C44-C46	σ*	0.01765	2.85	0.61
C1-C6	σ	1.9725	C1-C2	σ*	0.02372	3.63	1.26
C1-C6	σ	1.9725	C1-C44	σ*	0.03171	2.42	1.1

C1-C6	σ	1.9725	C2-H7	σ*	0.01683	2.62	1.13
C1-C6	σ	1.9725	C5-C6	σ*	0.01624	3.47	1.25
C1-C6	σ	1.9725	C5-H9	σ*	0.01458	2.24	1.12
C1-C6	σ	1.9725	C6-H10	σ*	0.01592	1.33	1.12
C1-C6	σ	1.9725	C44-H53	σ*	0.02173	0.69	1.1
C1-C44	σ	1.96707	C1-C2	σ*	0.02372	2.58	1.18
C1-C44	σ	1.96707	C1-C6	σ*	0.02727	2.41	1.16
C1-C44	σ	1.96707	C2-C3	σ*	0.02604	2.8	1.17
C1-C44	σ	1.96707	C5-C6	σ*	0.01624	1	1.17
C1-C44	σ	1.96707	C44-V45	σ*	0.01746	1	0.97
C1-C44	σ	1.96707	C44-C46	σ*	0.01765	1	0.97
C1-C44	σ	1.96707	C44-H53	σ*	0.02173	0.56	1.02
C1-C44	σ	1.96707	C45-H49	σ*	0.00628	1.29	1.01
C1-C44	σ	1.96707	C46-H52	σ*	0.00631	1.31	1.01
C2-C3	σ	1.97047	C1-C2	σ*	0.02372	4.32	1.26
C2-C3	σ	1.97047	C1-C44	σ*	0.03171	3.55	1.1
C2-C3	σ	1.97047	C2-H7	σ*	0.01683	1.32	1.13
C2-C3	σ	1.97047	C3-C4	σ*	0.02412	3.87	1.25
C2-C3	σ	1.97047	C3-C11	σ*	0.03717	2.27	1.09
C2-C3	σ	1.97047	C4-H8	σ*	0.016	2.54	1.12
C2-C3	σ	1.97047	C11-H14	σ*	0.02306	0.7	1.1
C2-H7	σ	1.97854	C1-C2	σ*	0.02372	1.17	1.08
C2-H7	σ	1.97854	C1-C6	σ*	0.02727	4.71	1.07
C2-H7	σ	1.97854	C2-C3	σ*	0.02604	1.02	1.07
C2-H7	σ	1.97854	C3-C4	σ*	0.02412	4.6	1.83
C3-C4	σ	1.9718	C2-C3	σ*	0.02604	3.9	1.25
C3-C4	σ	1.9718	C2-H7	σ*	0.01683	2.57	1.13
C3-C4	σ	1.9718	C3-C11	σ*	0.03717	2.31	1.1
C3-C4	σ	1.9718	C4-C5	σ*	0.01618	3.31	1.25
C3-C4	σ	1.9718	C4-H8	σ*	0.016	1.39	1.13
C3-C4	σ	1.9718	C5-H9	σ*	0.01458	2.22	1.13
C3-C4	σ	1.9718	C11-N17	σ*	0.04764	0.99	0.99
C3-C4	π	1.66846	C1-C2	π*	0.02372	18.69	0.29
C3-C4	π	1.66846	C5-C6	π*	0.32384	21.3	0.28
C3-C4	π	1.66846	C11-C12	σ*	0.02016	3.45	0.58
C3-C11	σ	1.97027	C11-N17	σ*	0.04764	3.25	0.55
C3-C11	σ	1.97027	C1-C2	σ*	0.02372	2.77	1.2
C3-C11	σ	1.97027	C2-C3	σ*	0.02604	2.44	1.19
C3-C11	σ	1.97027	C3-C4	σ*	0.02412	2.4	1.19
C3-C11	σ	1.97027	C4-C5	σ*	0.01618	2.43	1.19
C3-C11	σ	1.97027	C11-C12	σ*	0.02016	1.09	0.96
C3-C11	σ	1.97027	C11-H14	σ*	0.02306	0.59	1.04
C3-C11	σ	1.97027	C12-H15	σ*	0.01679	0.73	1.02
C4-C5	σ	1.97707	C3-C4	σ*	0.02412	3.67	1.26
C4-C5	σ	1.97707	C3-C11	σ*	0.03717	3.95	1.1
C4-C5	σ	1.97707	C4-H8	σ*	0.016	1.17	1.13
C4-C5	σ	1.97707	C5-C6	σ*	0.01624	2.97	1.26
C4-C5	σ	1.97707	C5-H9	σ*	0.01458	1.13	1.13
C4-C5	σ	1.97707	C6-H10	σ*	0.01592	2.48	1.13
C4-H8	σ	1.9793	C2-C3	σ*	0.02604	4.8	1.08
C4-H8	σ	1.9793	C3-C4	σ*	0.02412	0.94	1.08
C4-H8	σ	1.9793	C4-C5	σ*	0.01618	0.7	1.08
C4-H8	σ	1.9793	C5-C6	σ*	0.01624	3.76	1.08
C4-H8	σ	1.9793	C5-H9	σ*	0.01458	0.69	0.95
C5-C6	σ	1.97724	C1-C6	σ*	0.02727	3.77	1.25
C5-C6	σ	1.97724	C1-C44	σ*	0.03171	3.79	1.11
C5-C6	σ	1.97724	C4-C5	σ*	0.01618	2.96	1.26
C5-C6	σ	1.97724	C4-H8	σ*	0.016	2.5	1.13
C5-C6	σ	1.97724	C5-CH9	σ*	0.01458	1.18	1.13
C5-C6	σ	1.97724	C6-H10	σ*	0.01592	1.22	1.13

C5-C6	π	1.67845	C1-C2	π*	0.02372	21.46	0.29
C5-C6	π	1.67845	C3-C4	π*	0.35118	19.37	0.28
C5-H9	σ	1.97957	C1-C6	σ*	0.02727	4.22	1.07
C5-H9	σ	1.97957	C3-C4	σ*	0.02412	4.09	1.08
C5-H9	σ	1.97957	C4-C5	σ*	0.01618	0.62	1.08
C5-H9	σ	1.97957	C4-H8	σ*	0.016	0.69	0.95
C5-H9	σ	1.97957	C5-C6	σ*	0.01624	0.69	1.08
C5-H9	σ	1.97957	C6-H10	σ*	0.01592	0.72	0.95
C6-H10	σ	1.97898	C1-C2	σ*	0.02372	4.67	1.08
C6-H10	σ	1.97898	C1-C6	σ*	0.02727	0.97	1.07
C6-H10	σ	1.97898	C4-C5	σ*	0.01618	3.91	1.07
C6-H10	σ	1.97898	C5-C6	σ*	0.01624	0.72	1.08
C6-H10	σ	1.97898	C5-H9	σ*	0.01458	0.71	0.95
C11-C12	σ	1.96404	C3-C4	σ*	0.02412	0.84	1.15
C11-C12	σ	1.96404	C3-C4	π*	0.35118	2.52	0.62
C11-C12	σ	1.96404	C3-C11	σ*	0.03717	1.28	0.99
C11-C12	σ	1.96404	C11-H14	σ*	0.02306	0.59	1
C11-C12	σ	1.96404	C12-C13	σ*	0.03772	0.94	0.97
C11-C12	σ	1.96404	C12-H15	σ*	0.01679	0.6	0.99
C11-C12	σ	1.96404	C13-N18	σ*	0.01873	0.88	1.14
C11-C12	σ	1.96404	C13-C24	σ*	0.03308	4.19	1.09
C11-C12	σ	1.96404	N17-N18	σ*	0.02063	0.64	0.91
C11-C12	σ	1.96404	N17-H19	σ*	0.01585	2.47	1.01
C11-H14	σ	1.9747	C2-C3	σ*	0.02604	4.41	1.06
C11-H14	σ	1.9747	C12-C13	σ*	0.03772	0.95	0.89
C11-H14	σ	1.9747	C12-H15	σ*	0.01679	0.97	0.9
C11-H14	σ	1.9747	N17-N18	σ*	0.02063	2.15	0.82
C11-N17	σ	1.9848	C3-C4	σ*	0.02412	1.47	1.27
C11-N17	σ	1.9848	C3-C4	σ*	0.02412	1	0.74
C11-N17	σ	1.9848	C3-C11	σ*	0.03717	0.53	1.11
C11-N17	σ	1.9848	C12-H16	σ*	0.01218	0.99	1.11
C11-N17	σ	1.9848	C13-C24	σ*	0.03308	0.55	1.21
C12-C13	σ	1.97601	C3-C11	σ*	0.03717	0.62	1.02
C12-C13	σ	1.97601	C11-C12	σ*	0.02016	0.58	0.95
C12-C13	σ	1.97601	C11-H14	σ*	0.02306	1.05	1.03
C12-C13	σ	1.97601	C11-N17	σ*	0.04764	1.7	0.91
C12-C13	σ	1.97601	C12-H15	σ*	0.01679	0.59	1.01
C12-C13	σ	1.97601	C12-H16	σ*	0.01218	0.69	1.02
C12-C13	σ	1.97601	C13-N18	σ*	0.01873	0.85	1.17
C12-C13	σ	1.97601	C13-C24	σ*	0.03308	2.26	1.12
C12-C13	σ	1.97601	C23-C24	σ*	0.02539	2.77	1.17
C12-H15	σ	1.97035	C3-C11	σ*	0.03717	1.89	0.91
C12-H15	σ	1.97035	C11-H14	σ*	0.02306	1.12	0.92
C12-H15	σ	1.97035	C13-N18	σ*	0.01873	0.76	1.05
C12-H15	σ	1.97035	C13-N18	π*	0.24077	4.34	0.52
C12-H16	σ	1.97867	C11-N17	σ*	0.04764	1.11	0.81
C12-H16	σ	1.97867	C13-N18	σ*	0.01873	1.54	1.06
C12-H16	σ	1.97867	C13-N18	π*	0.24077	2.9	0.53
C13-N18	σ	1.98823	C12-C13	σ*	0.03772	1.06	1.26
C13-N18	σ	1.98823	C13-C24	σ*	0.03308	3.07	1.38
C13-N18	σ	1.98823	N17-H19	σ*	0.01585	1.12	1.3
C13-N18	σ	1.98823	C24-C25	σ*	0.02384	1.8	1.44
C13-N18	π	1.92351	C12-H15	σ*	0.01679	3.23	0.71
C13-N18	π	1.92351	C12-H16	σ*	0.01218	2.28	0.71
C13-N18	π	1.92351	C13-N18	π*	0.24077	1.17	0.33
C13-N18	π	1.92351	N17=H19	σ*	0.01585	1.22	0.73
C13-N18	π	1.92351	C24-C25	π*	0.39895	10.22	0.35
C13-C24	σ	1.967	C11-C12	σ*	0.02016	0.62	0.99
C13-C24	σ	1.967	C12-C13	σ*	0.03772	1.52	1.04
C13-C24	σ	1.967	C13-N18	σ*	0.01873	3.07	1.21

C13-C24	σ	1.967	N17-N18	σ*	0.02063	3.13	0.98
C13-C24	σ	1.967	C20-C25	σ*	0.01369	2.17	1.23
C13-C24	σ	1.967	C22-C23	σ*	0.01329	1.96	1.25
C13-C24	σ	1.967	C23-C24	σ*	0.02539	3.23	1.21
C13-C24	σ	1.967	C24-C25	σ*	0.02384	3.21	1.22
N17-N18	σ	1.98478	C11-H14	σ*	0.02306	0.5	1.2
N17-N18	σ	1.98478	C13-C24	σ*	0.03308	5.24	1.29
N17-H19	σ	1.98472	C11-C12	σ*	0.02016	1.24	0.97
N17-H19	σ	1.98472	C13-N18	σ*	0.01873	2.67	1.19
N17-H19	σ	1.98472	C13-N18	π*	0.24077	0.72	0.66
C20-C21	σ	1.9719	C20-C25	σ*	0.01369	3.43	1.27
C20-C21	σ	1.9719	C20-H26	σ*	0.014	1.31	1.13
C20-C21	σ	1.9719	C21-C22	σ*	0.0258	4.02	1.23
C20-C21	σ	1.9719	C21-N42	σ*	0.0339	2.01	1.11
C20-C21	σ	1.9719	C22-H27	σ*	0.01465	2.38	1.13
C20-C21	σ	1.9719	C25-H29	σ*	0.01427	2.08	1.13
C20-C21	σ	1.9719	C30-N42	σ*	0.02847	2.91	1.01
C20-C21	π	1.65361	C22-C23	π*	0.28711	15.84	0.29
C20-C21	π	1.65361	C24-C25	π*	0.39895	22.34	0.29
C20-C21	π	1.65361	C30-N42	σ*	0.02847	1.58	0.56
C20-C25	σ	1.97507	C13-C24	σ*	0.03308	3.63	1.19
C20-C25	σ	1.97507	C20-C21	σ*	0.02636	3.72	1.24
C20-C25	σ	1.97507	C20-H26	σ*	0.014	1.36	1.13
C20-C25	σ	1.97507	C21-N42	σ*	0.0339	4.26	1.11
C20-C25	σ	1.97507	C24-C25	σ*	0.02384	3.7	1.25
C20-C25	σ	1.97507	C25-H29	σ*	0.01427	1.12	1.13
C20-H26	σ	1.97686	C20-C21	σ*	0.02636	0.72	1.06
C20-H26	σ	1.97686	C20-C25	σ*	0.01369	0.94	1.09
C20-H26	σ	1.97686	C21-C22	σ*	0.0258	4.26	1.05
C20-H26	σ	1.97686	C21-N42	σ*	0.0339	0.69	0.94
C20-H26	σ	1.97686	C24-C25	σ*	0.02384	4.3	1.08
C20-H26	σ	1.97686	C25-H29	σ*	0.01427	0.74	0.95
C21-C22	σ	1.97094	C20-C21	σ*	0.02636	3.92	1.23
C21-C22	σ	1.97094	C20-H26	σ*	0.014	2.62	1.13
C21-C22	σ	1.97094	C21-N42	σ*	0.0339	1.91	1.11
C21-C22	σ	1.97094	C22-C23	σ*	0.01329	3.25	1.28
C21-C22	σ	1.97094	C22-H27	σ*	0.01465	1.18	1.12
C21-C22	σ	1.97094	C23-H28	σ*	0.01413	2.14	1.14
C21-C22	σ	1.97094	C31-N42	σ*	0.02576	3.52	1.01
C21-N42	σ	1.98351	C20-C21	σ*	0.40568	1.82	1.32
C21-N42	σ	1.98351	C20-C25	σ*	0.01369	1.39	1.35
C21-N42	σ	1.98351	C21-C22	σ*	0.0258	1.71	1.31
C21-N42	σ	1.98351	C22-C23	σ*	0.01329	1.39	1.37
C21-N42	σ	1.98351	C30-C33	σ*	0.02369	0.84	1.14
C21-N42	σ	1.98351	C30-N42	σ*	0.02847	0.98	1.09
C21-N42	σ	1.98351	C31-C32	σ*	0.02481	0.8	1.13
C21-N42	σ	1.98351	C31-N42	σ*	0.02576	0.97	1.1
C22-C23	σ	1.97599	C13-C24	σ*	0.03308	3.4	1.2
C22-C23	σ	1.97599	C21-C22	σ*	0.0258	3.53	1.23
C22-C23	σ	1.97599	C21-N42	σ*	0.0339	3.93	1.12
C22-C23	σ	1.97599	C22-H27	σ*	0.01465	1.42	1.14
C22-C23	σ	1.97599	C23-C24	σ*	0.02539	3.46	1.25
C22-C23	σ	1.97599	C23-H28	σ*	0.01413	1.2	1.16
C22-C23	σ	1.97599	C20-C21	π*	0.40568	20.93	0.27
C22-C23	σ	1.97599	C24-C25	π*	0.39895	16.57	0.28
C22-H27	σ	1.97706	C20-C21	σ*	0.02636	4.27	1.06
C22-H27	σ	1.97706	C21-C22	σ*	0.0258	0.6	1.05
C22-H27	σ	1.97706	C21-N42	σ*	0.0339	0.73	0.94
C22-H27	σ	1.97706	C22-C23	σ*	0.01329	1	1.1
C22-H27	σ	1.97706	C23-C24	σ*	0.02539	4.41	1.06

C22-H27	σ	1.97706	C23-H28	σ*	0.01413	0.74	0.97
C23-C24	σ	1.96968	C12-C13	σ*	0.03772	3.14	1.05
C23-C24	σ	1.96968	C13-C24	σ*	0.03308	3.55	1.17
C23-C24	σ	1.96968	C22-C23	σ*	0.01329	3.06	1.26
C23-C24	σ	1.96968	C22-H27	σ*	0.01465	2.39	1.11
C23-C24	σ	1.96968	C23-H28	σ*	0.01413	1.15	1.13
C23-C24	σ	1.96968	C24-C25	σ*	0.02384	3.99	1.23
C23-C24	σ	1.96968	C25-H29	σ*	0.01427	2.74	1.11
C23-H28	σ	1.97759	C21-C22	σ*	0.0258	4.74	1.04
C23-H28	σ	1.97759	C22-C23	σ*	0.01329	0.93	1.09
C23-H28	σ	1.97759	C22-H27	σ*	0.01465	0.86	0.94
C23-H28	σ	1.97759	C23-C24	σ*	0.02539	0.69	1.05
C23-H28	σ	1.97759	C24-C25	σ*	0.02384	4.44	1.06
C24-C25	σ	1.97235	C13-N18	σ*	0.01873	2.44	1.23
C24-C25	σ	1.97235	C13-C24	σ*	0.03308	3.53	1.18
C24-C25	σ	1.97235	C20-H26	σ*	0.014	3.25	1.26
C24-C25	σ	1.97235	C23-C24	σ*	0.02539	2.2	1.12
C24-C25	σ	1.97235	C23-H28	σ*	0.01413	3.98	1.23
C24-C25	σ	1.97235	C25-H29	σ*	0.01427	2.28	1.14
C24-C25	σ	1.97235	C25-H29	σ*	0.01427	1.26	1.12
C24-C25	π	1.65286	C13-N18	π*	0.24077	21.48	0.26
C24-C25	π	1.65286	C20-C21	π*	0.40568	18.75	0.27
C24-C25	π	1.65286	C22-23	π*	0.28711	20.57	0.28
C25-H29	σ	1.97859	C20-C21	σ*	0.02636	4.49	1.06
C25-H29	σ	1.97859	C20-C21	σ*	0.02636	0.79	1.09
C25-H29	σ	1.97859	C20-C25	σ*	0.01369	0.77	0.95
C25-H29	σ	1.97859	C20-H26	σ*	0.014	4.33	1.06
C25-H29	σ	1.97859	C23-C24	σ*	0.02539	0.7	1.07
C30-C33	σ	1.9864	C21-N42	σ*	0.0339	3.15	1.06
C30-C33	σ	1.9864	C30-H35	σ*	0.01113	0.71	1.03
C30-C33	σ	1.9864	C33-H36	σ*	0.01464	0.55	1.03
C30-H34	σ	1.98315	C21-N42	σ*	0.0339	0.66	0.93
C30-H34	σ	1.98315	C33-H37	σ*	0.02765	2.54	0.89
C30-H35	σ	1.9764	C31-N42	σ*	0.02576	3.83	0.85
C30-H35	σ	1.9764	C33-O43	σ*	0.02339	3.97	0.76
C30-N42	σ	1.97974	C20-C21	σ*	0.02636	2.28	1.26
C30-N42	σ	1.97974	C20-C21	π*	0.40568	0.89	0.74
C30-N42	σ	1.97974	C21-N42	σ*	0.0339	1.16	1.13
C30-N42	σ	1.97974	C31-H40	σ*	0.01226	1.12	1.1
C30-N42	σ	1.97974	C33-H36	σ*	0.01464	1	1.11
C31-C32	σ	1.98518	C21-N42	σ*	0.0339	3.25	1.06
C31-C32	σ	1.98518	C31-H40	σ*	0.01226	0.67	1.02
C31-C32	σ	1.98518	C32-H38	σ*	0.01466	0.54	1.03
C31-H40	σ	1.97582	C30-N42	σ*	0.02847	4.02	0.83
C31-H40	σ	1.97582	C32-O43	σ*	0.02339	4.24	0.76
C31-H41	σ	1.98413	C21-N42	σ*	0.0339	0.59	0.93
C31-H41	σ	1.98413	C32-H39	σ*	0.02764	2.39	0.89
C31-N42	σ	1.98345	C21-C22	σ*	0.0258	2.82	1.25
C31-N42	σ	1.98345	C21-N42	σ*	0.0339	1.2	1.14
C31-N42	σ	1.98345	C30-H35	σ*	0.01113	1.1	1.11
C31-N42	σ	1.98345	C30-N42	σ*	0.02847	0.56	1.03
C31-N42	σ	1.98345	C30-H35	σ*	0.01113	0.98	1.12
C32-H38	σ	1.98058	C31-N42	σ*	0.02576	3.53	0.84
C32-H38	σ	1.98058	C32-043	σ*	0.02339	3.5	0.76
C32-H39	σ	1.98748	C31-H41	σ*	0.03288	2.63	0.9
C32-043	σ	1.98987	C31-H40	σ*	0.01226	1.1	1.16
C32-043	σ	1.98987	C33-H36	σ*	0.01464	0.93	1.17
C33-H36	σ	1.98061	C31-N42	σ*	0.02576	3.64	0.83
C33-H36	σ	1.98061	C32-043	σ*	0.02339	3.47	0.76
C33-H37	σ	1.98749	C30-H34	σ*	0.03133	2.58	0.9

C33-O43	σ	1.98948	C30-H35	σ*	0.01113	1.2	1.16
C33-O43	σ	1.98948	C32-H38	σ*	0.01466	0.95	1.17
C44-C45	σ	1.97388	C1-C2	σ*	0.02372	1.61	1.16
C44-C45	σ	1.97388	C1-C2	π*	0.02372	2.11	0.63
C44-C45	σ	1.97388	C1-C44	σ*	0.03171	1.26	1
C44-C45	σ	1.97388	C44-C46	σ*	0.01765	0.69	0.95
C44-C45	σ	1.97388	C44-H53	σ*	0.02173	0.52	1.01
C44-C45	σ	1.97388	C45-H47	σ*	0.00585	0.51	1
C44-C45	σ	1.97388	C45-H49	σ*	0.00628	0.59	0.99
C44-C45	σ	1.97388	C46-H51	σ*	0.0058	1.65	1
C44-C46	σ	1.97313	C1-C2	σ*	0.02372	1.49	1.16
C44-C46	σ	1.97313	C1-C2	π*	0.02372	2.29	0.63
C44-C46	σ	1.97313	C1-C44	σ*	0.03171	1.26	1
C44-C46	σ	1.97313	C44-C45	σ*	0.01746	0.69	0.95
C44-C46	σ	1.97313	C44-H53	σ*	0.02173	0.52	1.01
C44-C46	σ	1.97313	C45-H47	σ*	0.00585	1.66	1
C44-C46	σ	1.97313	C46-H51	σ*	0.0058	0.51	1
C44-C46	σ	1.97313	C46-H52	σ*	0.00631	0.58	0.99
C44-H53	σ	1.96933	C1-C6	σ*	0.02727	4.84	1.03
C44-H53	σ	1.96933	C45-H48	σ*	0.00872	2.84	0.88
C44-H53	σ	1.96933	C46-H50	σ*	0.00865	2.83	0.88
C45-H47	σ	1.98907	C44-C46	σ*	0.01765	3.32	0.86
C45-H48	σ	1.98962	C44-H53	σ*	0.02173	2.63	0.91
C45-H49	σ	1.98786	C1-C44	σ*	0.03171	3.31	0.9
C46-H50	σ	1.98965	C44-H53	σ*	0.02173	2.63	0.91
C46-H51	σ	1.98902	C44-C45	σ*	0.01746	3.31	0.86
C46-H52	σ	1.98784	C1-C44	σ*	0.03171	3.27	0.9

in Fig. 8a-b and the charge transfer and excitation energy (E) eV are tabulated in Table-7. The Δr denotes the electron-hole distribution and the values depend on the overlap between electrons and holes. The larger Δr to the second excited state at 4.077 Å, compared to the first and third excited states 1.469 Å and 1.9546 Å, respectively. Similarly, the charge transfer length for the second excited states is larger than the first and third states. The blue clouded image in the molecule shows the holes distributed throughout the structure. The distribution of electrons was found in the pyrazole ring and the six-membered ring [34].

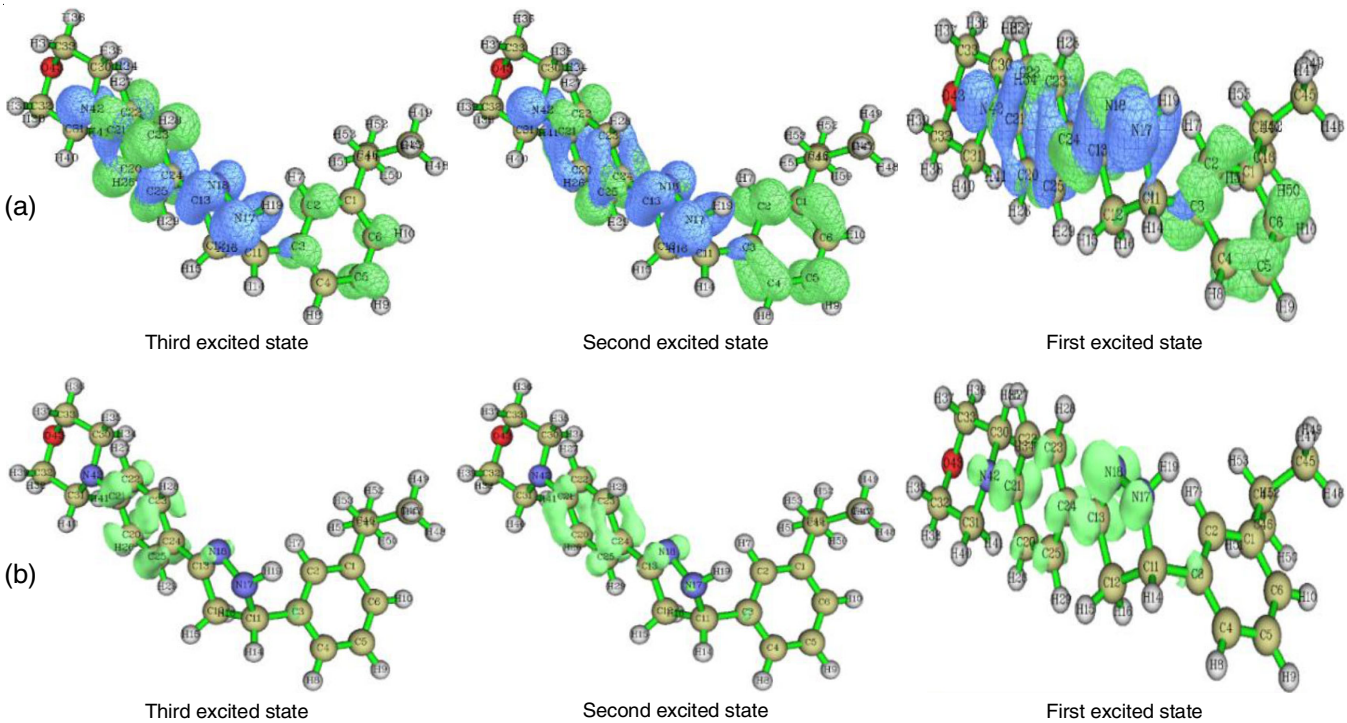

Fig. 8. (a) Electron-hole distribution (b) Electron-hole overlap for three excited states of titled molecule

TABLE-7
OVERLAP INTEGRAL, CHARGE TRANSFER LENGTH, Δr AND EXCITED ENERGY FOR DIFFERENT EXCITED STATES FOR TITLED MOLECULE

Excited state	Overlap integral of electron-hole (S)	Charge transfer length (D) (Å)	Δr (Å)	Excitation energy (E) (eV)
1	0.4069	2.0095	1.4698	3.8540
2	0.3091	2.5530	4.0770	4.2120
3	0.3485	1.0534	1.9546	4.2270

Electron localized function (ELF) and localized orbital locator (LOL) studies: The concept of electron localization in Lewis structures fundamentally depends on the principles of ELF τ(r) and LOL η(r). The electron localization function and localized orbital locator maps are based on the maximum number of electron pairs in molecular spacing due to covalent bonds. ELF and LOL elucidate the electron pair density and describe the intersection of maximum localized orbitals resulting from the gradients of orbitals, respectively. The blue colour region signifies the weak π-delocalized orbital and the low reddish blue colour symbolizes the strong π-delocalized orbitals. Weak π-delocalization has been perceived in the ring atoms of the molecule, namely C and H, while strong π-delocalization was prominent in oxygen atoms [1]. Hydrogen atoms present in the ring were observed to have strong electron localized function and also, the core electrons on heavy atoms are nitrogen and carbon (Fig. 9).

Docking studies: The drug-likeness of the molecules was determined through molecular docking studies by the interaction between the ligand and the protein. Prostate cancer was the targeted protein to study the inhibition of the molecules. The protein was retrieved from the online PDB databank and the PDB ID is 6XXO [35]. Their crystalline structure was reported with a resolution of 1.5 Å. The Autodock 2 software docked the protein and the ligand molecule and the PyMOL software captured their interactions [36]. Firstly, the Kollaman charge was added to stabilize the proteins, the water molecules were removed and the active sites were predicted through the Grid box technique [37].

From the docking score (Table-8), the titled molecule was considered the better ligand molecule to resist prostate cancer. The ligand interacts with the protein by nitrogen, hydrogen and oxygen and these atoms are considered to be the active region of the molecule. The targeted ligand was attached to isoleucine amino acid with a hydrogen bond. These results show that the synthesized molecule resist the carcinogenic pathogens through computational analysis. The 2D dock model and the Ramachandra plot depicted the protein-ligand interaction in Fig. 10b-c. From the 2D model, it was clear that isoleucine-59 was pi-sigma bonded with the compound.

ADME studies: The synthesized compound exhibits the pharmacokinetic, physico-chemical, lipophilicity and drug-likeness properties. These properties were predicted using the Swiss-ADME web tool [38]. The molecule has four rotatable bonds and 26 heavy atoms with a topological polar surface area (TPSA) of 36.86 $Å^2$. The sp^3 carbon atoms were predicted with a proportion of 0.41; the structure has one hydrogen bond donor and two hydrogen bond acceptors, suggesting moderate saturation. These hydrogen bonds help the docking studies, creating the interaction between the protein and ligand. The lipophilicity value log $P_{o/w}$ of 3.63 signifies that the molecule has a strong affinity for lipids, indicating its suitability for oral administration and its superior absorption and distribution properties. The boiled egg graph (Fig. 11) and the pharmacokinetics data (Fig. 12) give valid results about the ability to penetrate the BBB [39]. In addition to passing the Ghose, Veber, Egan and Muegge filters and Lipinski's rule of five without any infractions, it also exhibits advantageous drug-like qualities. At 0.55, the bioavailability score is considered moderate. The synthetic accessibility score was recorded to be 3.73, which suggests a moderate level of synthetic complexity. These results give insight into oral delivery and absorption and distribution

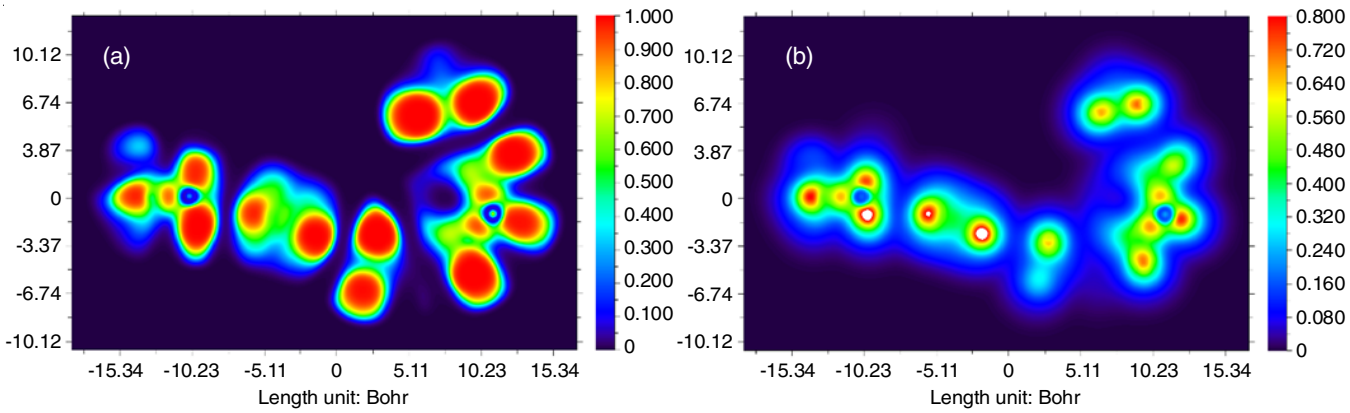

Fig. 9. (a) ELF and (b) LOL colour mapping of titled molecule

TABLE-8
DOCKING STUDIES OF TITLED MOLECULE AGAINST PROSTATE CANCER

Protein ID (PDB ID)	Type of protein	Ligands	Binding energy (Kcal/mol)	Bonded residues	Number of hydrogen bond	Bond distance (Å)
6XXO	Prostate cancer	Titled molecule	-7.3	ILE-59	1	4.5

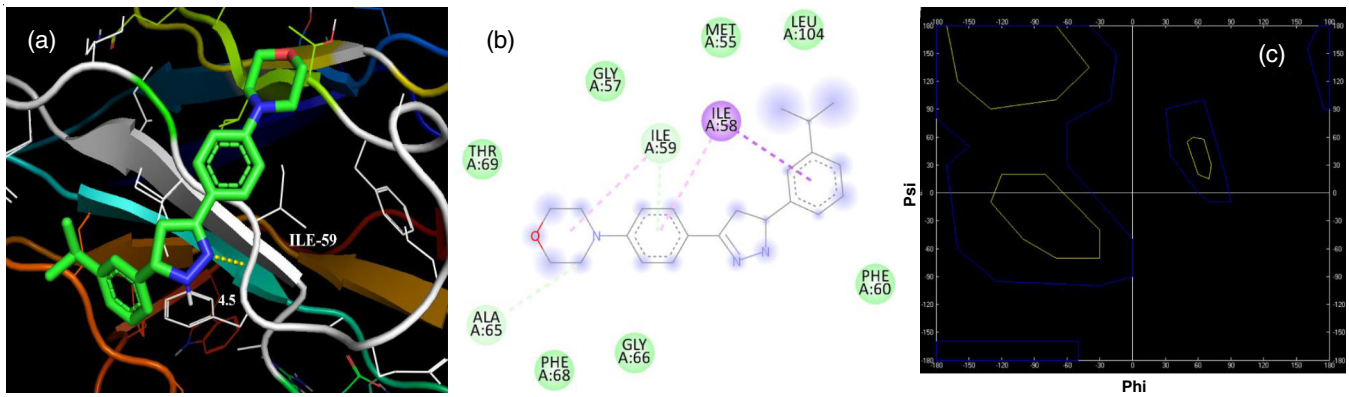

Fig. 10. 3D docking image of titled molecule (a), 2D interaction image (b) and Ramachandra plot (c)

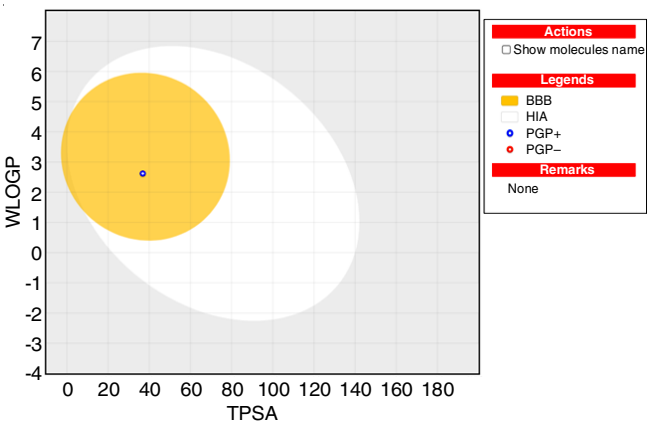

Fig. 11. Boiled egg model for the titled molecule retrieved from SwissADME

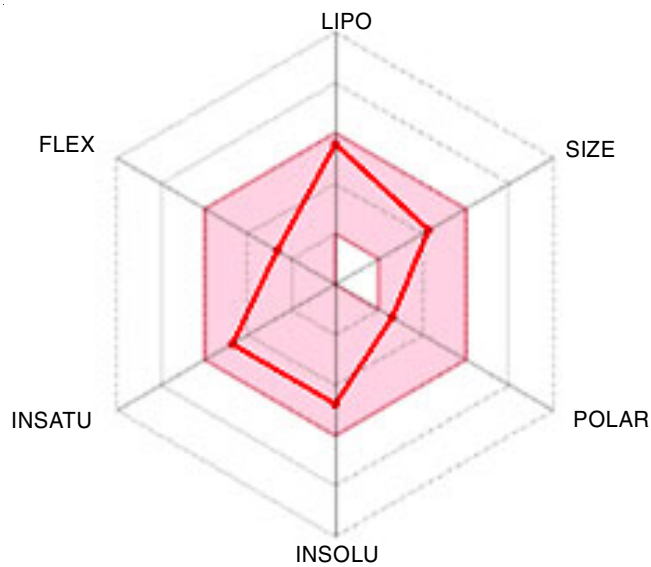

Fig. 12. Representing the outcomes of titled compound for the ADME data

properties, which also perfectly suit the docking studies and also have drug likeness ability.

Conclusion

The new biologically active 4-(4-(4,5-dihydro-5-(4-isopropylphenyl)-1*H*-pyrazol-3-yl)phenyl)morpholine was synthesized and characterized using several techniques and correlated using DFT studies. The FT-IR spectrum confirmed the successful synthesis of the target molecule, which was also ideally suited to the theoretical FT-IR analysis. The bond length of C-C of the target molecule was calculated to be 1.4 Å, which was also in remarkable agreement with the experimental data. The ^{1}H and ^{13}C NMR have also confirmed the successful synthesis and the UV-Vis spectra, the molecule exhibits λ_{max} at 320 nm, which shows the high optical behaviour of molecule. The theoretically calculated HOMO and LUMO show a band gap of around 4.2 eV and act as a stable compound. Further, NBO and MEP give effective results about the acceptor-donor and nucleophilicity of the synthesized molecule. The docking studies show effective results against prostate cancer with a docking score of -7.3 Kcal/mol. The ADME studies give valid results about the drug-likeness of the molecule. The NLO studies show the optoelectronic property of the molecule.

ACKNOWLEDGEMENTS

The authors acknowledge the Quantum Computational Research Laboratory (QCR-Lab) in St. Joseph's College of Arts & Science (Autonomous), Cuddalore, India, for the computational studies.

CONFLICT OF INTEREST

The authors declare that there is no conflict of interests regarding the publication of this article.

REFERENCES

1. A. Kumari and R.K. Singh, *Bioorg. Chem.*, **96**, 103578 (2020); https://doi.org/10.1016/j.bioorg.2020.103578
2. F. Arshad, M.F. Khan, W. Akhtar, M.M. Alam, L.M. Nainwal, S.K. Kaushik, M. Akhter, S. Parvez, S.M. Hasan and M. Shaquiquzzaman, *Eur. J. Med. Chem.*, **167**, 324 (2019); https://doi.org/10.1016/j.ejmech.2019.02.015
3. R. Lesyk, *J. Med. Sci.*, **89**, 407 (2020); https://doi.org/10.20883/medical.e407
4. S. El-Assaly, A.E.H.A. Ismail, H. Bary and M. Abouelenein, *Curr. Chem. Lett.*, **10**, 309 (2021); https://doi.org/10.5267/j.ccl.2021.3.003
5. R. Thomas, Y.S. Mary, K.S. Resmi, B. Narayana, B.K. Sarojini, G. Vijayakumar and C. Van Alsenoy, *J. Mol. Struct.*, **1181**, 455 (2019); https://doi.org/10.1016/j.molstruc.2019.01.003
6. S. Sebastian, S. Sylvestre, N. Sundaraganesan, B. Karthikeyan and S. Silvan, *Heliyon*, **8**, e08821 (2022); https://doi.org/10.1016/j.heliyon.2022.e08821

7. K.A. Abdalkarim, S.J. Mohammed, A.H. Hasan, K.M. Omer, K.H.H. Aziz, F. Paularokiadoss, R.F. Hamarouf, H.Q. Hassan and T. Christopher Jeyakumar, *Chem. Phy. Imp.*, **8**, 100402 (2024); https://doi.org/10.1016/j.chphi.2023.100402
8. S.S. Margreat, S. Ramalingam, H.M. Al-Maqtari, J. Jamalis, S. Sebastian, S. Periandy and S. Xavier, *Chem. Data Coll.*, **33**, 100701 (2021); https://doi.org/10.1016/j.cdc.2021.100701
9. C. Adaikalaraj D. Bhakiaraj R.N. Asha, T.A. Sandosh, S. Manivarman and F. Paularokiadoss, *Vietnam J. Chem.*, **60**, 472 (2022); https://doi.org/10.1002/vjch.202100193
10. H.K. Thabet, A.F. Al-Hossainy and M. Imran, *Opt. Mater.*, **105**, 109915 (2020); https://doi.org/10.1016/j.optmat.2020.109915
11. A. Frisch, Gaussian 09W Reference, Gaussian Inc., Wallingford CT, USA, pp. 1-25 (2009).
12. H. Kruse, L. Goerigk and S. Grimme, *J. Org. Chem.*, **77**, 10824 (2012); https://doi.org/10.1021/jo302156p
13. M.H. Jamróz. *Spectrochim. Acta A: Mol. Biomol. Spectrosc.*, **114**, 220 (2013); https://doi.org/10.1016/j.saa.2013.05.096
14. R. Tiwari, K. Mahasenan, R. Pavlovicz, C. Li and E. Tjarks, *J. Chem. Inf. Mol.*, **49**, 1581 (2009); https://doi.org/10.1021/ci900031y
15. Z. Ullah, B. Mustafa, H.J. Kim, Y.S. Mary, Y. Shyma Mary and H.W. Kwon, *J. Mol. Liq.*, **357**, 119076 (2022); https://doi.org/10.1016/j.molliq.2022.119076
16. P. Botschwina and J. Flügge, *Chem. Phys. Lett.*, **180**, 589 (1991); https://doi.org/10.1016/0009-2614(91)85015-O
17. J. Demaison, L. Margules and J.E. Boggs, *Chem. Phys.*, **260**, 65 (2000); https://doi.org/10.1016/S0301-0104(00)00253-6
18. S.K. Saha, A. Hens, N.C. Murmu and P. Banerjee, *J. Mol. Liq.*, **215**, 486 (2016); https://doi.org/10.1016/j.molliq.2016.01.024
19. J.M. Ramos, O. Versiane, J. Felcman and C.A. Téllez S., *Spectrochim. Acta: Mol. Biomol. Spectrosc.*, **72**, 182 (2009); https://doi.org/10.1016/j.saa.2008.09.026
20. Y. Kaddouri, F. Abrigach, N. Mechbal, Y. Karzazi, M. El Kodadi, A. Aouniti and R. Touzani, *Mater. Today Proc.*, **13**, 956 (2019); https://doi.org/10.1016/j.matpr.2019.04.060
21. R.R. Pillai, V.V. Menon, Y.S. Mary, S. Armakovic, S.J. Armakovic and C.Y. Panicker, *J. Mol. Struct.*, **1130**, 208 (2017); https://doi.org/10.1016/j.molstruc.2016.10.032
22. S.S. Pathade, V.A. Adole, B.S. Jagdale and T.B. Pawar, *J. Mater. Sci. Res. India*, **17**, 27 (2020); https://doi.org/10.13005/msri.17.special-issue1.05
23. N. Manju, B. Kalluraya, Asma and M.S. Kumar, *J. Mol. Struct.*, **1193**, 386 (2019); https://doi.org/10.1016/j.molstruc.2019.05.049
24. K. Bhavani, J. Christina Rhoda, M.K. Hossain and C. Karnan, *Opt. Mater.*, **148**, 114924 (2024); https://doi.org/10.1016/j.optmat.2024.114924
25. C. Morell, A. Grand and A. Toro-Labbe, *J. Phys. Chem. A*, **109**, 205 (2005); https://doi.org/10.1021/jp046577a
26. M. Arivazhagan, S. Manivel, S. Jeyavijayan and R. Meenakshi, *Spectrochim. Acta Part A: Mol. Biomol. Spectros.*, **134**, 493 (2015); https://doi.org/10.1016/j.saa.2014.06.108
27. B.A. Shainyan, N.N. Chipanina, T.N. Aksamentova, L.P. Oznobikhina, G.N. Rosentsveig and I.B. Rosentsveig, *Tetrahedron*, **66**, 8551 (2010); https://doi.org/10.1016/j.tet.2010.08.076
28. K. Anbukarasi, S. Xavier, J. Jamalis, S. Sebastian, F. Paularokiadoss, S. Periandy and R. Rajkumar, *J. Mol. Struct.*, **1249**, 131580 (2022); https://doi.org/10.1016/j.molstruc.2021.131580
29. K. Anbukarasi, S. Xavier, A.H. Hasan, Y.L. Er, J. Jamalis, S. Sebastian and S. Periandy, *Curr. Phys. Chem.*, **13**, 37 (2023); https://doi.org/10.2174/1877946812666220928102954
30. A. Innasiraj, B. Anandhi, Y. Gnanadeepam, N. Das, F. Paularokiadoss, A.V. Ilavarasi, C.D. Sheela, D.R. Ampasala and T.C. Jeyakumar, *J. Mol. Struct.*, **1265**, 133450 (2022); https://doi.org/10.1016/j.molstruc.2022.133450
31. J. Jamalis, S. Sebastian, S.S. Margreat, K. Subashini, S. Ramalingam, H.M. Al-Maqtari, S. Periandy and S. Xavier, *Chem. Data Coll.*, **28**, 100415 (2020); https://doi.org/10.1016/j.cdc.2020.100415
32. S. Demir, F. Tinmaz, N. Dege and I.O. Ilhan, *J. Mol. Struct.*, **1108**, 637 (2016); https://doi.org/10.1016/j.molstruc.2015.12.057
33. S. Asokan, S. Sebastian, B. Karthikeyan, S. Xavier, R.G. Raman, S. Silvan, S.S. Margreat and R. Sagayaraj, *Chem. Phys. Impact*, **8**, 100497 (2024); https://doi.org/10.1016/j.chphi.2024.100497
34. S. Sebastian, S. Sylvestre, N. Sundaraganesan, B. Karthikeyan and S. Silvan, *Heliyon*, **8**, e08821 (2022); https://doi.org/10.1016/j.heliyon.2022.e08821
35. L. Rosenfeld, A. Sananes, Y. Zur, S. Cohen, K. Dhara, S. Gelkop, E. Ben Zeev, A. Shahar, L. Lobel, B. Akabayov, E. Arbely and N. Papo, *J. Med. Chem.*, **63**, 7601 (2020); https://doi.org/10.1021/acs.jmedchem.0c00418
36. W.L. DeLano, *CCP4 Newsl. Protein Crystallogr.*, **40**, 82 (2002).
37. P. Ayaz, D. Andres, D.A. Kwiatkowski, C.C. Kolbe, P. Lienau, G. Siemeister, U. Lücking and C.M. Stegmann, *ACS Chem. Biol.*, **11**, 1710 (2016); https://doi.org/10.1021/acschembio.6b00074
38. A. Daina, O. Michielin and V. Zoete, *Sci. Rep.*, **7**, 42717 (2017); https://doi.org/10.1038/srep42717
39. P. Pritha, G. Kishore, S. Xavier, F. Paularokiadoss, D. Bhakiaraj, S. Periandy, G. Bouzid and S. Ayachi, *Mater. Chem. Phys.*, **326**, 129829 (2024); https://doi.org/10.1016/j.matchemphys.2024.129829